Journal of Power Sources 187 (2009) 324–331

Contents lists available at ScienceDirect

Journal of Power Sources

journal homepage: www.elsevier.com/locate/jpowsour

Performance decay of proton-exchange membrane fuel cells under open circuit conditions induced by membrane decomposition

Seiho Sugawara[a,b,*], Takao Maruyama[a], Yoshiki Nagahara[a], Shyam S. Kocha[a], Kazuhiko Shinohra[a], Kohei Tsujita[b], Shigenori Mitsushima[b], Ken-ichiro Ota[b]

[a] Fuel Cell Laboratory, Nissan Research Center, Nissan Motor Co., Ltd., 1 Natsushima-cho, Yokosuka, Kanagawa 237-8523, Japan
[b] Chemical Energy Laboratory, Yokohama National University, 79-5 Tokiwadai, Hodogaya-ku, Yokohama, Kanagawa 240-8501, Japan

ARTICLE INFO

Article history:
Received 22 September 2008
Received in revised form 7 November 2008
Accepted 7 November 2008
Available online 17 November 2008

Keywords:
Proton-exchange membrane fuel cell
Open circuit
Oxygen reduction reaction
Membrane decomposition
Anion adsorption
Cyclic voltammetry

ABSTRACT

The degradation in performance of proton-exchange membrane fuel cells (PEMFCs) under open circuit conditions was investigated. The oxygen reduction reaction (ORR) kinetic current density at 0.9 V was found to decrease from 36 to 4 mA cm^{-2} (geometric) without significant crossover increase or loss in the electrochemically active surface area. Cyclic voltammograms for the electrodes show characteristic changes, e.g. appearance of peaks at ~0.2 V and shift of the onset of platinum oxide formation to higher potentials. It was identified that the large ORR kinetic decay has its origins in the reduction of available Pt sites due to adsorption of anions, which are postulated to be membrane decomposition products such as sulfate ions. Procedures carried out to condense water in the fuel cell led to the expulsion of anions out of the membrane electrode assembly (MEA) resulting in the partial recovery of ORR kinetic current density to 15 mA cm^{-2}. In order to attain complete performance recovery of the catalyst, a more effective and practical method to flush out the anions is desirable.

1. Introduction

One of major barriers to the commercialization of proton-exchange membrane fuel cells (PEMFCs) for transportation power sources is the degradation issue of membrane electrode assemblies (MEAs) [1–3]. Unlike stationary applications, PEMFCs for automotive applications are operated under a variety of modes which can be divided broadly into start/stop, load cycling, and low load.

During start-up, when hydrogen is introduced into the anode where air is already present, the electrode potential of the portion of the cathode opposite the part of the anode where oxygen is remaining can exceed 1.5 V, causing carbon corrosion [4–6]. A similar phenomenon is also observed during shut-down. The carbon corrosion causes aggregation of catalyst particles and insufficient electric contact between carbon agglomerates, resulting in a decrease of the electrochemically active surface area (ECA) of the catalyst. Hydrophobicity and structure of electrode are also subject to harmful effects so that the gas transport property of the MEA diminishes. This is one of the most severe degradation that a PEMFC can experience. Over the last few years, a combination of more benign operating conditions during start-up and shut-down such as low temperature and low RH, use of advanced materials such as graphitized carbon support, and low anode loading have greatly diminished the issues.

In the course of vehicle operation, the fuel cell experiences roughly 300,000 load cycles between peak power and idle over its life [2]. Although the anode potential will settle in a narrow range close to the reversible hydrogen potential because the hydrogen reaction has a very high exchange current density on platinum, the cathode potential fluctuates widely, approximately between 0.6 and 1.0 V. Under such condition, cathode ECA decreases rapidly due to platinum dissolution [7–13] although carbon corrosion is minimal. Darling and Meyers [8,9] developed mathematical models in which rapid anodic potential transition exposes bare platinum to corrosive potential before a protective oxide layer forms on the surface of platinum. The platinum dissolution can be mitigated by modifying potential cycling profiles [14], lowering temperature and RH, and use of modified catalysts such as Pt-alloy and larger particle Pt.

The low load operating mode, which mainly consists of idling and open circuit conditions, is known to accelerate proton-exchange membrane (PEM) decomposition especially under low humidification [15–22]. The decomposition of PEM is caused by attack of peroxi-radicals which originate from hydrogen peroxide produced at the anode catalyst surface due to reactant hydrogen and oxygen crossover from the cathode side [15,18]. Ohma et al. [23,24]

* Corresponding author at: Fuel Cell Laboratory, Nissan Research Center, Nissan Motor Co., Ltd., 1 Natsushima-cho, Yokosuka, Kanagawa 237-8523, Japan. Tel.: +81 46 867 5331; fax: +81 46 867 5332.
E-mail address: seihou-sugawara@mail.nissan.co.jp (S. Sugawara).

0378-7753/$ – see front matter © 2008 Elsevier B.V. All rights reserved.
doi:10.1016/j.jpowsour.2008.11.021

suggested a mechanism in which platinum particles deposited in the membrane, referred to as the Pt band, promotes peroxide formation. This mechanism can explain an observation of the membrane degradation with MEA which is catalyzed only on the cathode side [19].

The membrane decomposition causes an increase of gas crossover and a voltage drop especially at low current densities. Further propagation of the membrane decomposition eventually causes a steep increase of gas crossover, which results in a catastrophic performance drop of the PEMFC and an inevitable shut-down of the PEMFC power plant system. Lifetime of a membrane is often defined as the time at which a steep increase of gas crossover beyond an acceptable limit is observed. Significant efforts to improve the lifetime of membranes are being made [25–27].

Unlike the above definition of the lifetime of a membrane, lifetime of an MEA or PEMFC is practically defined as the time when the power density decay approaches a certain value such as 10% of initial [28,29]. The lifetime of an MEA is generally shorter than that of the membrane. In other words, power density drops by 10% before a steep increase of gas crossover. If the cause of power density decay under low load operating mode is not the membrane degradation, improvement of the lifetime of membrane will not always improve the lifetime of MEA.

Although many papers on membrane degradation and gas crossover increase under the low load operation mode or open circuit condition have been published [15–24], there are only a few reports on fuel cell performance change under these operation modes [30,31]. Inaba et al. [30] reported that voltage drop under low load (0.3 A cm^{-2}) operation at low humidification is due to dehydration of the membrane and the ionomer in the catalyst layers; both cause an increase of ohmic losses while the latter causes a decrease in electrode activity which is mostly recoverable. There are also several reports on the significant decay of open circuit voltage (OCV) observed in open circuit endurance tests [16–18,21–24]. Under open circuit conditions, there is no external current or load so that ohmic losses are unlikely to be a factor causing the large OCV decay. Therefore, we suspect that other mechanisms might play an important role in the OCV decay mechanism. However, taking into consideration the large drop of open circuit voltage observed in the open circuit endurance operation [16–18,21–24], since there is no external current and only small internal current due to crossover and shorting at the condition, other mechanisms may play a role.

The main objective of this study is to carefully examine the fuel cell performance loss under open circuit conditions at low humidity and investigate the underlying root mechanisms involved. In addition, procedures for performance recovery are also explored.

2. Experimental

2.1. MEA and cell preparation

Electrocatalyst layers were fabricated on polytetrafluoroethylene (PTFE) sheets by screen printing of catalyst ink. The catalyst ink was prepared by mixing carbon-supported Pt catalyst (TEC10E50E, TKK, Japan), ionomer solution (Nafion® DE 2020, DuPont, USA), propylene glycol, and water. The electrocatalyst layers were transferred on a perfluorosulfonic acid (PFSA) membrane (Nafion® NRE-212, DuPont, USA) by hot-press to fabricate a catalyst-coated membrane (CCM) with 25 cm^2 active area. The chemical structure of Nafion is shown in Fig. 1. The Pt loading was maintained at 0.34 mg cm^{-2} for both anode and cathode. The CCM was sandwiched between two commercially available carbon paper gas diffusion layers with hydrophobic microporous layer to obtain an MEA. Single cells were assembled using serpentine flow fields with channels machined into graphite blocks. The MEA was conditioned at 80 °C and a constant current density of 1 A cm^{-2} for 13.5 h with

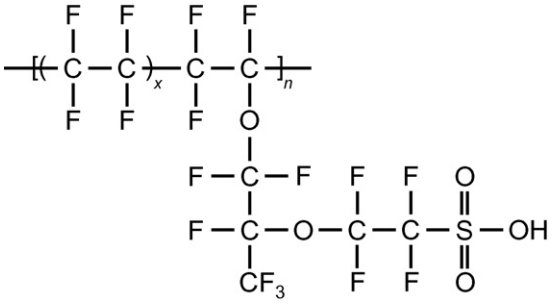

Fig. 1. Chemical structure of Nafion.

1.0 dm^3 min^{-1} of hydrogen and 1.0 dm^3 min^{-1} of air for anode and cathode feed, respectively (100% RH).

2.2. Open circuit endurance operation

Fuel cell test stations from Chino Corporation (Japan) were employed for all experiments. During open circuit duration, the anode flow field was supplied with 0.5 dm^3 min^{-1} of hydrogen and the cathode flow field was supplied with 0.5 dm^3 min^{-1} of air. Back-pressure was maintained at ambient. Cell temperature was controlled at 90 °C and temperature of bubbler type humidifier for both anode and cathode were controlled at 61.2 °C in order to set the gas RH at 30%. The duration of the open circuit test was 48 h. Cell voltage (open circuit voltage) and area specific resistance measured using high frequency (1 kHz) resistance meter (Model 3566, Tsuruga Electric, Japan) were monitored during the period. Effluent water was collected and fluoride and sulfate ions were analyzed using ion chromatography.

2.3. Diagnosis

Diagnostic tests were conducted before and after the endurance test in order to determine performance change. Polarization curves were taken starting from open circuit to high current density along with area specific resistance measurements. Hydrogen and air were used as reactant gases and constant utilization of 0.67 and 0.5 were set respectively. Temperature of the humidifier for anode and cathode were controlled at 58.9 °C and 71.4 °C in order to set gas relative humidity at 40% and 70%, respectively. Back-pressure was maintained at ambient. Cell temperature was controlled at 80 °C. Oxygen was also used at a low utilization of 10% for the cathode feed to minimize effect of concentration drop and focus on kinetic loss.

ECA of the cathode catalyst layer was measured by in-situ cyclic voltammetry (CV) using potentiostats (HZ-3000, Hokuto Denko). Cell temperature was kept at 80 °C for the CV measurement in order to avoid variation of conditions as much as possible. The anode was fed with fully humidified hydrogen at 0.5 dm^3 min^{-1} serving as reference/counter electrode. The cathode was fed with fully humidified nitrogen at 0.5 dm^3 min^{-1} serving as working electrode. Voltammograms were measured within a scan range of 0.04–0.9 V at a scan rate of 50 mV s^{-1}. The ECA can be usually calculated by integration of the total charge of hydrogen desorption using the specific capacitance of 210 μC cm^{-2}. However, at the set temperature 80 °C, it is very difficult to estimate real absolute value of the surface area [32]. Hence, relative value of the ECA was calculated by division of hydrogen desorption total charge by one measured before the endurance test.

Hydrogen crossover (HXO) and electronic shorting were electrochemically measured by steady-state potentiostatic method. Potential was held at 0.2, 0.3, 0.4, and 0.5 V for 180 s for each potential. Other conditions were the same as that of CV. Measured current represents leak current consisting of both the HXO and the short-

ing. The currents during the final 20 s of each potential hold were averaged. A plot of the average current vs potential typically gave a straight line. The HXO current density and the short-circuit resistance were determined from the intercept and the slope of the straight line, respectively.

2.4. Recovery operation

Based on analyses of the diagnostic results (see next section for details), a water condensation operation was selected as the recovery operation. The anode flow field was supplied with 0.5 $dm^3\,min^{-1}$ of hydrogen and the cathode flow field was supplied with 0.5 $dm^3\,min^{-1}$ of nitrogen. The cell temperature was controlled at 50 °C and the humidifier temperature was controlled at 80 °C so that water can be condensed in the cell. This condition with leaving open circuit was maintained for 2 h. A typical open circuit voltage in the condition is ~0.1 V. The effluent water was collected and fluoride and sulfate were analyzed during the recovery operation as well.

3. Results and discussion

3.1. Observation during open circuit operation

Fig. 2 shows the decay trends for OCV and area specific resistance during the open circuit endurance test. The OCV gradually decreased from 0.99 to 0.87 V. In contrast, the area specific resistance did not show significant change. The theoretical OCV corresponds to the difference between the equilibrium potentials of hydrogen oxidation reaction (HOR) and oxygen reduction reaction (ORR), i.e. 1.229 V at standard conditions. Under operating conditions, the OCV usually deviates from the theoretical value mainly due to not only the difference of reactant partial pressures and temperature from standard conditions but also mixed cathode potential arising mainly from reactions [33–35]:

$$O_2 + 4H^+ + 4e^- \rightarrow 2H_2O \quad (1)$$

$$H_2 \rightarrow 2H^+ + 2e^- \quad (2)$$

$$Pt + H_2O \rightarrow PtO + 2H^+ + 2e^- \quad (3)$$

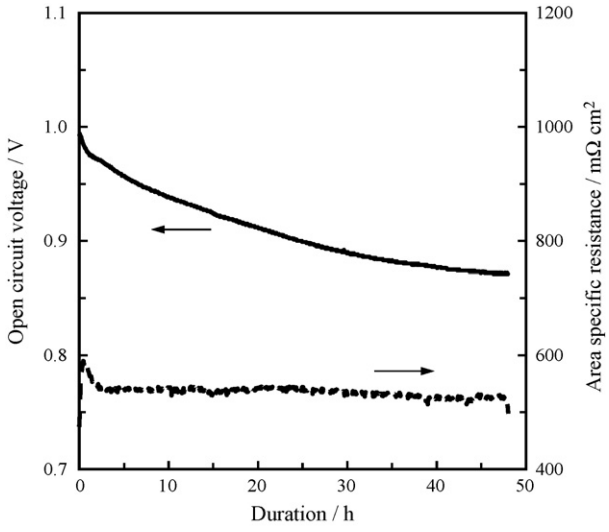

Fig. 2. Change of the open circuit voltage (solid line) and area specific resistance (dotted line) measured by high frequency (1 kHz) resistance meter vs time under open circuit operation at 80 °C with H_2 on the anode and air on the cathode. Reactants were humidified at 61.2 °C to regulate the relative humidity to 30%.

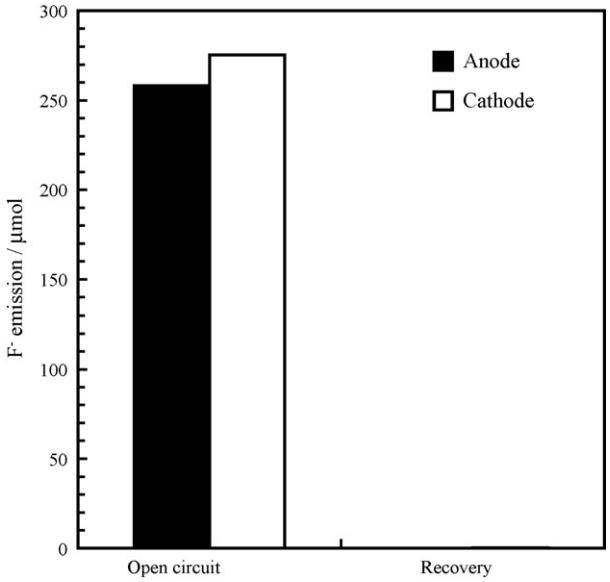

Fig. 3. Total fluoride emission under the open circuit operation (48 h) and the recovery operation (2 h) in effluent water analyzed using ion chromatography.

Hence, the observed decay of the OCV can be considered to originate from (1) decay of ORR kinetics, (2) increase of the HXO, and (3) change of reaction rate for formation/reduction of Pt surface oxide or other processes such as dissolution/re-deposition of Pt, adsorption/desorption of impurities, and corrosion of carbon support. The HXO determined by electrochemical diagnosis conducted before and after the open circuit operation showed only slight increase from 1.51 to 1.58 mA cm^{-2}. Pt surface oxide growth at potentiostatic condition usually proceeds according to logarithmic oxide growth kinetics [36,37] at potentials near OCV. This implies that the Pt surface oxidation rate should be diminishing. Consequently, the decay of OCV is most likely due to ORR kinetics decay.

Fluoride emission and sulfate emission under the open circuit operation are shown in Figs. 3 and 4. Although the HXO did not increase significantly, large amount (~530 μmol by summing up the both electrode) of fluoride in the effluent water was detected,

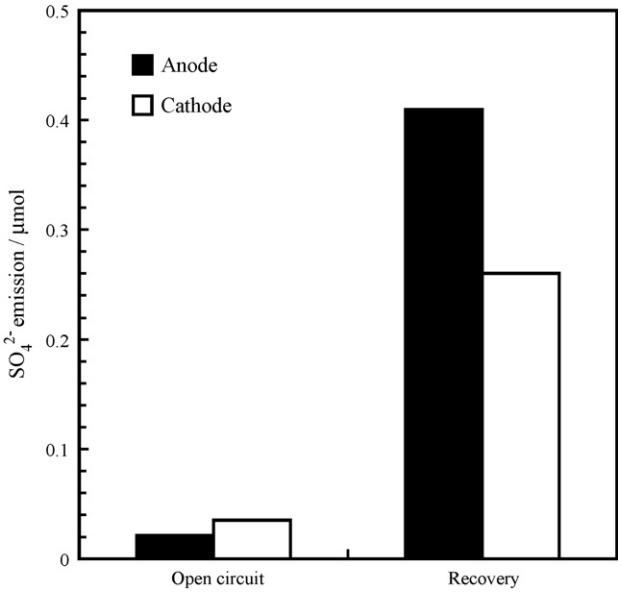

Fig. 4. Total sulfate emission under the open circuit operation (48 h) and the recovery operation (2 h) in effluent water analyzed by ion chromatography.

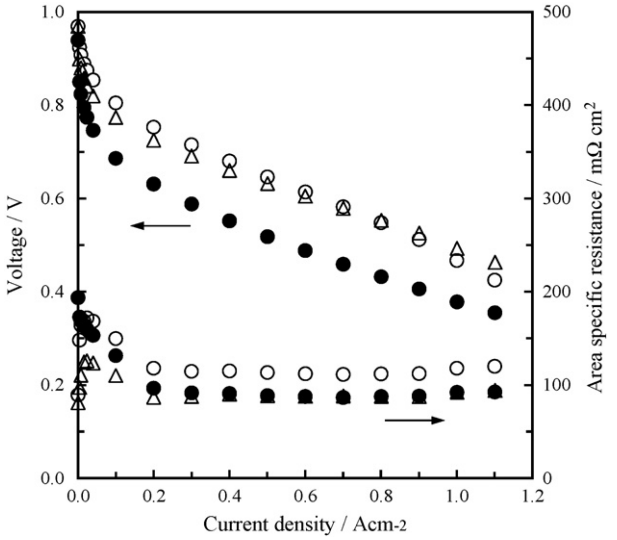

Fig. 5. Polarization curves with area specific resistances for H_2/air operation at constant utilization of 67/10% (40/70% RH) and 80 °C cell temperature measured before the open circuit operation (open circles), after the open circuit operation (solid circles), and after the recovery operation (triangles).

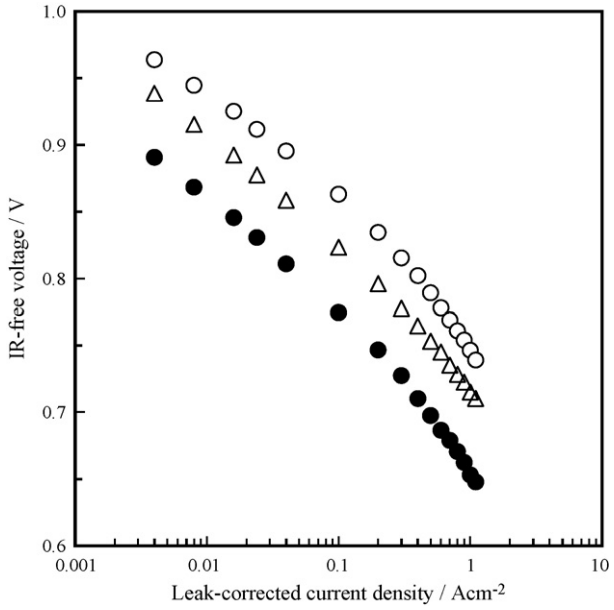

Fig. 6. Tafel plots for H_2/O_2 operation at constant utilization of 67/10% (40/70% RH) and 80 °C cell temperature measured before the open circuit operation (open circles), after the open circuit operation (solid circles), and after the recovery operation (triangles).

indicating the membrane was chemically decomposing. By a rough estimation using Nafion's general chemical structure (Fig. 1) and typical value for the properties of Nafion NRE-212 such as 50.8 μm thickness, 100 g m^{-2} basis weight, and 0.92 meq. g^{-1} acid capacity [38], 6% of fluorine in membrane was released. On the other hand, sulfate emission during the open circuit operation was relatively low (Fig. 3).

3.2. Analyses based on diagnostic results

Change of polarization curve along with area specific resistances measured utilizing H_2/air as reactant gases is shown in Fig. 5. A large voltage decay in the whole current density range can be observed. This voltage decay is not due to membrane dehydration because the measured area specific resistance actually decreased after the open circuit operation. Mass transfer characteristics were not affected by the open circuit operation because a noticeable voltage drop at high current density was not observable.

Fig. 6 shows the change of IR-free, leak-corrected, Tafel plots measured employing H_2/O_2 as reactant gases. In order to extract the ORR kinetic current from the measured current, the correction of the leak current due to HXO and the electrical shorting was carried out using following equation:

$$i_{lc} = i + i_{HXO} + \frac{V}{r_s} \quad (4)$$

where i_{lc} is the leak-corrected current density, i is the measured current density, i_{HXO} is the HXO current density, V is the cell voltage, and r_s is the area specific shorting resistance [39].

Since the voltage decay is roughly independent of current density, increase of kinetic loss is obvious. The kinetic loss increase is a function of the deterioration of catalytic activity, which consists of area specific activity and roughness factor. The current density at 0.9 V (IR-free) derived from interpolation or extrapolation of the plots decreased from 36 to 4 mA cm^{-2} (geometric), as shown in Fig. 7.

Figs. 8 and 9 show comparison of cyclic voltammograms of the anode and the cathode, respectively. Voltammograms for both the anode and the cathode exhibit a similar transformation of their profiles when measured before and after the open circuit operation. Paying attention to H_{upd} region ($0.1 < E < 0.4$ V) of the voltammograms, no significant loss of electrochemically active surface area is found because curves are roughly overlap before and after the endurance test. In fact, the final ECA of the cathode relative to the initial value is ~0.85. Therefore, the principal cause of the kinetic loss increase is a result of the lowering of the catalyst specific activity rather than loss of roughness factor.

By comparing the shapes of the voltammograms carefully, characteristic changes such as appearance of peaks at ~0.2 V can be observed. Furthermore, shifts of the onset of platinum oxide formation to higher potentials and the appearances of small peaks at ~0.45 V can be observed in Figs. 8 and 9. Similar changes of voltammogram have been reported in the literature to be caused by specifically adsorbing anions on polycrystalline and single crystal Pt [40–45]. Hence, we can infer it is estimated that the adsorb-

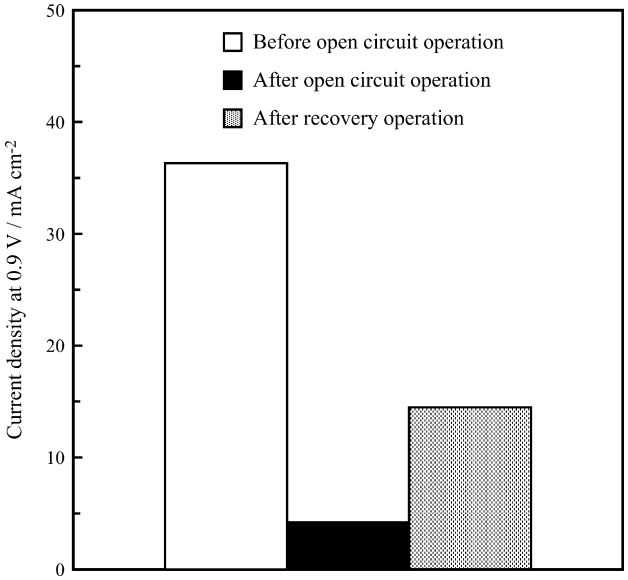

Fig. 7. Comparison of current density at 0.9 V (IR-free) derived from Fig. 3 by interpolation or extrapolation.

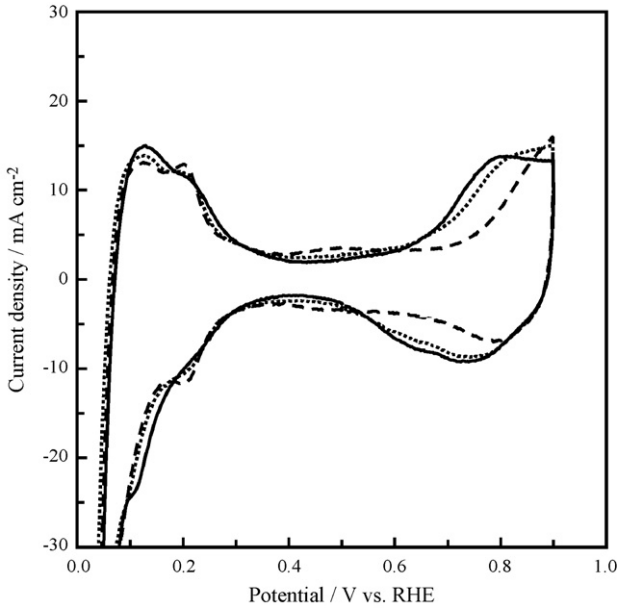

Fig. 8. Cyclic voltammograms of the anode measured before the open circuit operation (solid line), after the open circuit operation (dashed line), and after the recovery operation (dotted line). All curves are measured at 80 °C cell temperature, 50 mV s^{-1} scan rate. The anode was fed with fully humidified N_2 at 0.5 dm^3 min^{-1} serving as working electrode. The cathode was fed with fully humidified H_2 at 0.5 dm^3 min^{-1} serving as reference/counter electrode.

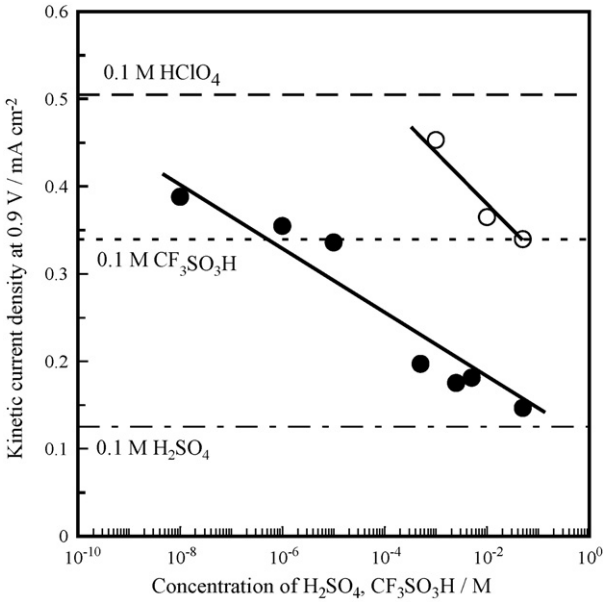

Fig. 10. Oxygen reduction reaction kinetic current density at 0.9 V vs RHE in 0.1 M $HClO_4$ containing H_2SO_4 (solid circles) or CF_3SO_3H (open circles) at various concentrations at 25 °C [63,64]. The dashed, dotted, and dash–dot lines represent the kinetic current density in unmixed electrolytes.

ing anion produced by membrane decomposition is likely to have caused the change in the voltammograms. Among various decomposition products of membrane such as fluoride, sulfate, and other fragments of perfluorosulfonic acid [17,30,46], the most suspicious one as a cause of voltammogram change is sulfate because its adsorption strength is known to be high. In addition, remaining amount of sulfate within the MEA is expected to be relatively large since the release of sulfate ions during the open circuit operation is much lower than that of fluoride ions (Figs. 3 and 4). Inaba et al. [30] reported that the sulfate ions accumulate in the MEA during low humidification operation at low current density (300 mA cm^{-2}) although fluoride ions can be released in the form of volatile HF molecules.

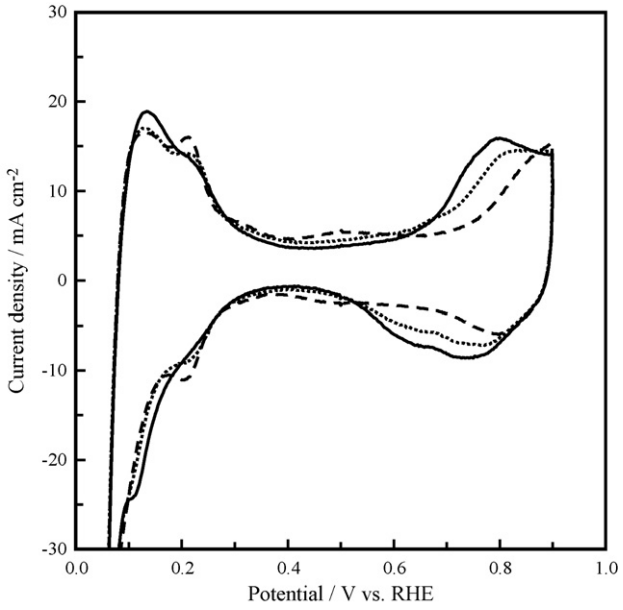

Fig. 9. Cyclic voltammograms of the cathode measured before the open circuit operation (solid line), after the open circuit operation (dashed line), and after the recovery operation (dotted line). All curves are measured at 80 °C cell temperature, 50 mV s^{-1} scan rate. The cathode was fed with fully humidified N_2 at 0.5 dm^3 min^{-1} serving as working electrode. The anode was fed with fully humidified H_2 at 0.5 dm^3 min^{-1} serving as reference/counter electrode.

The equilibrium potential of HOR/HER (0 V) is low enough for anions not to adsorb on Pt except for extremely strong adsorbing one such as I^- [47] and Br^- [48,49]. Thus, we can expect that the HOR is not suppressed by the adsorbing anions produced by decomposition of the membrane like sulfate whose surface concentration on Pt at this potential region is very low [43,47,50–52]. Although one report showed sulfate ions diminished HOR [53], intrinsic activity of Pt for HOR is much higher than that for ORR so that the impact of adsorbing anion on the fuel cell performance is likely to be insignificant.

On the other hand, many reports have shown that the presence of adsorbing anions significantly affect the ORR activity on polycrystalline Pt [42,54,55], Pt single crystal [43,56–59], and carbon-supported Pt nano-particle [60–62]. Tsujita et al. [63,64] investigated influence of a trace of sulfate ion and trifluoromethane sulfonate ion on ORR activity employing RRDE setup with Pt polycrystalline disk electrode (Fig. 10). As shown in Fig. 10, sulfate addition to non-adsorbing electrolyte (0.1 M $HClO_4$) suppressed 20% of ORR activity even at sulfate concentration as low as 10^{-8} M. The significance of the sulfate ion on the ORR activity compared with other perfluorocarboxylic acids has been confirmed by Kabasawa et al. [65]. Therefore, the kinetic loss increase observed here in the open circuit operation can be also attributed to the ORR activity lowering due to the presence of adsorbing anions, probably sulfate, formed by decomposition of the membrane.

Schmidt et al. [62] have reported that the amount of peroxide formation is almost the same in 0.5 M $HClO_4$ and 0.5 M H_2SO_4 at potentials positive to the hydrogen adsorption region. In contrast, Tsujita et al. [63,64] reported an increase in H_2O_2 formation at typical operating potentials caused by the presence of sulfate ions at higher concentration than 10^{-6} M (Fig. 11). It implies that the sul-

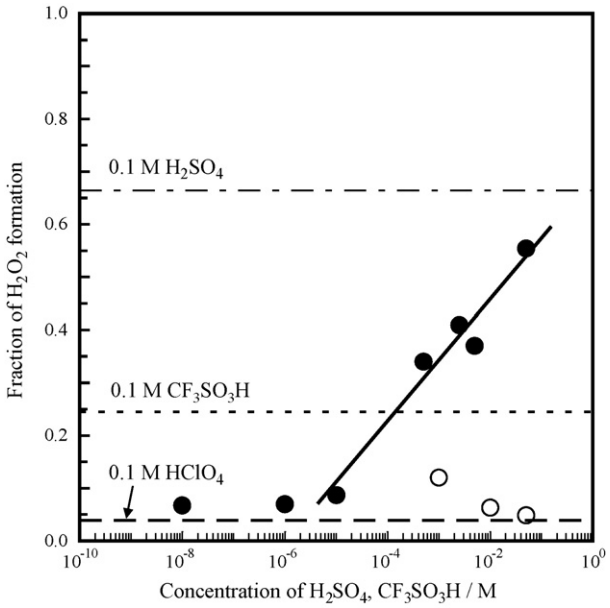

Fig. 11. Fraction of H_2O_2 formation at 0.6 V vs RHE in 0.1 M $HClO_4$ containing H_2SO_4 (solid circles) or CF_3SO_3H (open circles) at various concentrations at 25 °C [63,64]. The dashed, dotted, and dash–dot lines represent the fraction in unmixed electrolytes.

fate ions produced by decomposition of membrane is capable of accelerating decomposition of the membrane.

3.3. Recovery of performance

Based on the analyses described above, we presumed that the kinetic loss increase under the open circuit operation can be attributed to the presence of adsorbing anions, such as sulfate ion. Nagahara et al. [66] reported on the impact of SO_2 on PEMFC performance and found that the severe performance loss due to decrease of available Pt sites by adsorption of sulfur species can be partially recovered by excursions to high potentials (>0.9 V) where the sulfur species can be oxidized to sulfate. They also found that the specific adsorption of sulfate is a cause of residual performance loss and complete recovery can be achieved only by flushing out of sulfate from the catalyst layer by an application of 100% RH operation at 1 A cm^{-2} using pure oxygen for the cathode feed.

The performance loss under the open circuit operation reported in this paper is also expected to be recovered by the flushing out of sulfate. However, pure oxygen is typically unavailable in fuel cell vehicles. The 100% RH operation utilizing air cannot be implemented because liquid water easily obstructs transport of oxygen unless flow rates are extraordinarily high. Here, we employed a water condensation operation as an alternative recovery operation for flushing out sulfate ions because there are opportunities for water to be condensed when the temperature of the fuel cell stack falls after shut-down of the FCV. As described in Section 2, gases humidified at 80 °C were supplied to the cell which is controlled at 50 °C in order to condense water in it. N_2 was used for the cathode feed instead of air so as to isolate and examine the effect of only water condensation although it is also unavailable in the vehicle. This condition was maintained for 2 h.

In Figs. 3 and 4, total fluoride and sulfate emission during the recovery operation are shown along with that during open circuit operation. Very small amounts (<1 μmol) of fluoride emission during the recovery operation were detected, indicating almost no membrane decomposition during the operation. However, large amounts of sulfate were detected in the effluent water during the recovery operation. Hence, it was confirmed that the open circuit operation caused membrane decomposition resulting in the formation of sulfate ions which accumulated within MEA during the open circuit period and was exhausted out of the MEA during the recovery period.

In Figs. 8 and 9, transition of the cyclic voltammogram during the condensation operation is shown. The voltammogram of the anode shows almost complete restoration to its initial shape whereas the cathode shows only partial recovery. The extent of recovery corresponds to the amount of sulfate exhausted out of the MEA (Fig. 4).

Figs. 5 and 6 show partial restoration of performance by the recovery operation, which is consistent with the partial recovery of voltammogram. The ORR current density at 0.9 V (IR-free) increased to 15 mA cm^{-2} (geometric), as shown in Fig. 7. In order to attain full recovery, a more effective method to wash out the sulfate like the application of 100% RH operation at 1 A cm^{-2} using oxygen for the cathode feed is needed [66]. However, as mentioned above, this method is not practical. Finding new uncomplicated method is desired.

3.4. Hypothesis for degradation mechanism

The rate of the ORR can be expressed as [58]:

$$i = nFkc_{O_2}(1-\theta_{ad})^x \exp\left(\frac{-\beta FE}{RT}\right)\exp\left(\frac{-\gamma r\theta_{ad}}{RT}\right) \quad (5)$$

where i is the ORR current, n is the number of electrons, k is the rate constant, c_{O_2} is the concentration of O_2, θ_{ad} is the total surface coverage by adsorbed species, x is the site requirement of the adsorbates, β and γ are the symmetry factors, F is the Faraday's constant, E is the potential, R is the gas constant, T is the temperature, and r is the Temkin parameter. With the existence of adsorbing anions such as sulfate,

$$\theta_{ad} = \theta_{OHad} + \theta_{Aad} \quad (6)$$

where θ_{OHad} is the surface coverage by the hydroxyl species, and θ_{Aad} is the surface coverage by the adsorbing anions. It is expected that θ_{ad} after the open circuit operation is higher than that of initial value. Fig. 12 shows correlation between platinum

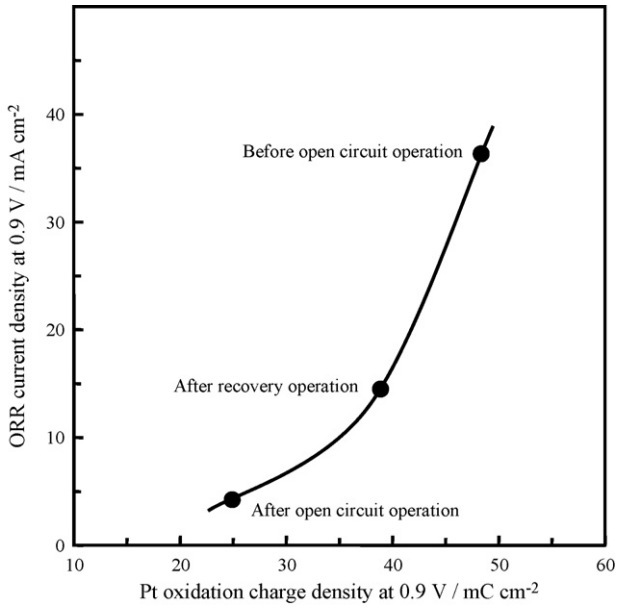

Fig. 12. Correlation between platinum oxidation charge density at 0.9 V and ORR current density at 0.9 V.

oxidation charge density at 0.9 V, which was derived by integration of oxidation current density from onset to 0.9 V in cyclic voltammograms, and ORR current density at 0.9 V. In this figure, the Pt oxidation charge, which is representative of θ_{OHad}, is low after the open circuit operation. It indicates enormous effect of the coverage by the anion θ_{Aad} on the ORR kinetics after the open circuit operation.

The mechanism of the performance decay by the open circuit operation can be postulated as follows:

- Electrolyte fragments form as a result of membrane decomposition.
- Specifically adsorbing anions such as sulfate in the electrolyte fragments accumulate within MEA.
- The anions cause loss of available Pt sites for oxygen reduction resulting in performance loss.
- The anions may accelerate formation of H_2O_2 that leads to further decomposition of the membrane.
- Expulsion of the anions out of MEA by washing out can recover the performance.

4. Conclusions

We investigated the fuel cell performance change under open circuit condition under low humidity in order to determine the cause of performance change. Large losses in ORR kinetic activity were observed based on diagnostic tests conducted before and after open circuit operation. The profile of cyclic voltammograms obtained during diagnosis revealed appearance of peaks at ~0.2 V and shifts of the onset of platinum oxide formation that correspond to adsorption of anions such as sulfate ions. The anions are postulated to be membrane decomposition products. Ion chromatography analyses of the effluent water during the open circuit operation indicated large amount of fluoride ions but not a corresponding amount of sulfate ions. It was hypothesized that the sulfate ions are trapped in the MEA and adsorb on the platinum sites. This coverage of platinum site by anions results in a loss in ORR activity. Flushing out of the trapped anions in the MEA by water condensation led to a partial recovery of ORR activity. In order to attain complete recovery, a more effective and practical method to flush out the anions is required.

References

[1] D.P. Wilkinson, J. St-Pierre, in: W. Vielstich, H.A. Gasteiger, A. Lamm (Eds.), Handbook of Fuel Cells: Fundamentals, Technology and Applications, vol. 3, Wiley, New York, 2003, pp. 611–626.
[2] M.F. Mathias, R. Makharia, H.A. Gasteiger, J.J. Conley, T.J. Fuller, C.J. Gittleman, S.S. Kocha, D.P. Miller, C.K. Mittelsteadt, T. Xie, S.G. Yan, P.T. Yu, Electrochem. Soc. Interface 14 (3) (2005) 24–35.
[3] R. Borup, J. Meyers, B. Pivovar, Y.S. Kim, R. Mukundan, N. Garland, D. Myers, M. Wilson, F. Garzon, D. Wood, P. Zelenay, K. More, K. Stroh, T. Zawodzinski, J. Boncella, J.E. McGrath, M. Inaba, K. Miyatake, M. Hori, K. Ota, Z. Ogumi, S. Miyata, A. Nishikata, Z. Siroma, Y. Uchimoto, K. Yasuda, K. Kimijima, N. Iwashita, Chem. Rev. 107 (2007) 3904–3951.
[4] C.A. Reiser, L. Bregoli, T.W. Patterson, J.S. Yi, J.D. Yang, M.L. Perry, T.D. Jarvi, Electrochem. Solid-State Lett. 8 (2005) A273–A276.
[5] J.P. Meyers, R.M. Darling, J. Electrochem. Soc. 153 (2006) A1432–A1442.
[6] H. Tang, Z. Qi, M. Ramani, J.F. Elter, J. Power Sources 158 (2006) 1306–1312.
[7] T. Patterson, in: G.J. Igwe, D. Mah (Eds.), Fuel Cell Technology Topical Conference Proceedings, AIChE, New York, 2002, pp. 313–318.
[8] R.M. Darling, J.P. Meyers, J. Electrochem. Soc. 150 (2003) A1523–A1527.
[9] R.M. Darling, J.P. Meyers, J. Electrochem. Soc. 152 (2005) A242–A247.
[10] X. Wang, R. Kumar, D.J. Myers, Electrochem. Solid-State Lett. 9 (2006) A225–A227.
[11] K. Yasuda, A. Taniguchi, T. Akita, T. Ioroi, Z. Siroma, Phys. Chem. Chem. Phys. 8 (2006) 746–752.
[12] R.L. Borup, J.R. Davey, F.H. Garzon, D.L. Wood, M.A. Inbody, J. Power Sources 163 (2006) 76–81.
[13] S. Mitsushima, S. Kawahara, K. Ota, N. Kamiya, J. Electrochem. Soc. 154 (2007) B153–B158.
[14] M. Uchimura, S. Kocha, ECS Trans. 11 (1) (2007) 1215–1226.
[15] A.B. LaConti, M. Hamdan, R.C. McDonald, in: W. Vielstich, H.A. Gasteiger, A. Lamm (Eds.), Handbook of Fuel Cells: Fundamentals, Technology and Applications, vol. 3, Wiley, New York, 2003, pp. 647–662.
[16] E. Endoh, S. Terazono, H. Widjaja, Y. Takimoto, Electrochem. Solid-State Lett. 7 (2004) A209–A211.
[17] K. Teranishi, K. Kawata, S. Tsushima, S. Hirai, Electrochem. Solid-State Lett. 9 (2006) A475–A477.
[18] M. Inaba, T. Kinumoto, M. Kiriake, R. Umebayashi, A. Tasaka, Z. Ogumi, Electrochim. Acta 51 (2006) 5746–5753.
[19] V.O. Mittal, H.R. Kunz, J.M. Fenton, Electrochem. Solid-State Lett. 9 (2006) A299–A302.
[20] A. Collier, H. Wang, X.Z. Yuan, J. Zhang, D.P. Wilkinson, Int. J. Hydrogen Energy 31 (2006) 1838–1854.
[21] A. Ohma, S. Suga, S. Yamamoto, K. Shinohara, J. Electrochem. Soc. 154 (2007) B757–B760.
[22] A. Ohma, S. Yamamoto, K. Shinohara, ECS Trans. 11 (1) (2007) 1181–1192.
[23] A. Ohma, S. Suga, S. Yamamoto, K. Shinohara, ECS Trans. 3 (1) (2006) 519–529.
[24] A. Ohma, S. Yamamoto, K. Shinohara, J. Power Sources 182 (2008) 39–47.
[25] D.E. Curtin, R.D. Lousenberg, T.J. Henry, P.C. Tangeman, M.E. Tisack, J. Power Sources 131 (2004) 41–48.
[26] E. Endoh, ECS Trans. 3 (1) (2006) 9–18.
[27] L. Merlo, A. Ghielmi, L. Cirillo, M. Gebert, V. Arcella, J. Power Sources 171 (2007) 140–147.
[28] U.S. Department of Energy (DOE), Hydrogen, Fuel Cells & Infrastructure Technologies Program, Multi-Year Research, Development and Demonstration Plan, 2007, http://www1.eere.energy.gov/hydrogenandfuelcells/mypp/.
[29] New Energy and Industrial Technology Development Organization (NEDO), http://www.nedo.go.jp/nenryo/index.html.
[30] M. Inaba, H. Yamada, R. Umebayashi, M. Sugishita, A. Tasaka, Electrochemistry 75 (2007) 207–212.
[31] J. Yu, T. Matsuura, Y. Yoshikawa, M.N. Islam, M. Hori, Electrochem. Solid-State Lett. 8 (2005) A156–A158.
[32] M. Uchimura, S.S. Kocha, In: AIChE Annual Meeting Abstracts, AIChE, 2007, Abstract no. 295b.
[33] J. Zhang, Y. Tang, C. Song, J. Zhang, H. Wang, J. Power Sources 163 (2006) 532–537.
[34] G. Tian, S. Wasterlain, I. Endichi, D. Candusso, F. Harel, X. Francois, M. Pera, D. Hissel, J. Kauffman, J. Power Sources 182 (2008) 449–461.
[35] N. Yousfi-Steiner, Ph. Moçotéguy, D. Candusso, D. Hissel, A. Hernandez, A. Aslanides, J. Power Sources 183 (2008) 260–274.
[36] B.E. Conway, Prog. Surf. Sci. 49 (1995) 331–452.
[37] M. Alsabet, M. Grden, G. Jerkiewicz, J. Electroanal. Chem. 589 (2006) 120–127.
[38] Product Information, DuPont™ Nafion® PFSA Membranes, NRE-211 and NRE-212, DuPont Fuel Cells, Wilmington.
[39] S.S. Kocha, in: W. Vielstich, H.A. Gasteiger, A. Lamm (Eds.), Handbook of Fuel Cells: Fundamentals, Technology and Applications, vol. 3, Wiley, New York, 2003, pp. 538–565.
[40] P. Zelenay, M. Gamboa-Aldeco, G. Horanyi, A. Wieckowski, J. Electroanal. Chem. 357 (1993) 307–326.
[41] D.R. Lawson, L.D. Whiteley, C.R. Martin, J. Electrochem. Soc. 135 (1988) 2247–2253.
[42] H. Saffarian, P. Ross, F. Behr, G. Gard, J. Electrochem. Soc. 139 (1992) 2391–2397.
[43] M.E. Gamboa-Aldeco, E. Herrero, P.S. Zelenay, A. Wieckowski, J. Electroanal. Chem. 348 (1993) 451–457.
[44] N. Markovic, H. Gasteiger, P.N. Ross, J. Electrochem. Soc. 144 (1997) 1591–1597.
[45] A. Capon, R. Parsons, J. Electroanal. Chem. 39 (1972) 275–286.
[46] J. Healy, C. Hayden, T. Xie, K. Olson, R. Waldo, M. Brundage, H. Gasteiger, J. Abbott, Fuel Cells 5 (2005) 302–308.
[47] J.O. Bockris, M. Gamboa-Aldeco, M. Szklarczyk, J. Electroanal. Chem. 339 (1992) 355–400.
[48] N.M. Markovic, C.A. Lucas, H.A. Gasteiger, P.N. Ross, Surf. Sci. 365 (1996) 229–240.
[49] N. Garcia-Araez, V. Climent, E. Herrero, J. Feliu, J. Lipkowski, J. Electroanal. Chem. 591 (2006) 149–158.
[50] K. Kunimatsu, M.G. Samant, H. Seki, J. Electroanal. Chem. 258 (1989) 163–177.
[51] W. Savich, S. Sun, J. Lipkowski, A. Wieckowski, J. Electroanal. Chem. 388 (1995) 233–237.
[52] E. Herrero, J. Mostany, J.M. Feliu, J. Lipkowski, J. Electroanal. Chem. 534 (2002) 79–89.
[53] E. Lamy-Pitara, S. El Mouahid, J. Barbier, Electrochim. Acta 45 (2000) 4299–4308.
[54] K.-L. Hsueh, E.R. Gonzalez, S. Srinivasan, Electrochim. Acta 28 (1983) 691–697.
[55] E. Yeager, M. Razaq, D. Gervasio, A. Razaq, D. Tryk, in: D. Scherson, D. Tryk, M. Daroux, X. Xing (Eds.), Proceedings of the Workshop on Structural Effects in Electrocatalysis and Oxygen Electrochemistry, vol. 92–11, The Electrochemical Society, Pennington, 1992, pp. 440–473.
[56] H. Kita, Y. Gao, K. Ohnishi, Chem. Lett. 23 (1994) 73–76.
[57] H. Kita, H. Lei, Y. Gao, J. Electroanal. Chem. 379 (1994) 407–414.
[58] N.M. Markovic, H.A. Gasteiger, B.N. Grgur, P.N. Ross, J. Electroanal. Chem. 467 (1999) 157–163.
[59] V. Stamenkovic, N.M. Markovic, P.N. Ross, J. Electroanal. Chem. 500 (2001) 44–51.
[60] G. Tamizhmani, J.P. Dodelet, D. Guay, J. Electrochem. Soc. 143 (1996) 18–23.

[61] U.A. Paulus, T.J. Schmidt, H.A. Gasteiger, R.J. Behm, J. Electroanal. Chem. 495 (2001) 134–145.
[62] T.J. Schmidt, U.A. Paulus, H.A. Gasteiger, R.J. Behm, J. Electroanal. Chem. 508 (2001) 41–47.
[63] K. Tsujita, S. Sugawara, S. Mitsushima, K. S Ota, Proceedings of the 17th Denkyoku-Zairyo-Kenkyukai The Committee of the Electrolytic Science and Technology, The Electrochemical Society of Japan, Tokyo, 2007, pp. 29–32.
[64] K. Tsujita, S. Sugawara, S. Mitsushima, K. Ota, Proceedings of the Fall Meeting of the Electrochemical Society of Japan, Tokyo, 2007, p. 9.
[65] A. Kabasawa, H. Uchida, M. Watanabe, Electrochem. Solid-State Lett. 11 (2008) B190–B192.
[66] Y. Nagahara, S. Sugawara, K. Shinohara, J. Power Sources 182 (2008) 422–428.